Modeling of geometric configuration and fiber interactions in short fiber reinforced composites via new modified Eshelby tensors and enhanced mean-field homogenization

E. Rashidinejad[1,*], H. Ahmadi[1], M. Hajikazemi[1,2], W. Van Paepegem[1]

[1]*Department of Materials, Textiles and Chemical Engineering, Faculty of Engineering and Architecture, Ghent University, Technologiepark Zwijnaarde 46, Ghent, Belgium*

[2]*Dutch Polymer Institute (DPI), P.O. Box 902, 5600 AX, Eindhoven, The Netherlands*

Abstract

Determination of the effective elastic properties of unidirectional short fiber reinforced composites (SFRCs) is a key fundamental requirement which is usually estimated by mean-field homogenization (MFH) methods. Available classical MFH methods only account for volume fraction and aspect ratio of the fibers and do not capture the realistic interactions between closely spaced short fibers since they cannot consider the physical geometry of the fibers nor their packing configurations. In this work, new modified Eshelby tensors associated with an enhanced MFH are developed which resolve the mentioned limitations of the available MFH methods and preserve their computational efficiency. While classical Eshelby tensors used in MFHs depend only on the aspect ratio of the fictitious ellipsoidal inclusion and material properties of the matrix, the introduced modified Eshelby tensors additionally account for physical cylindrical geometry as well as interactions of the short fibers with different packing configurations. Moreover, non-uniform homogenizing eigenstrains required for accurate homogenization of the short fibers are also incorporated by the proposed analytical treatment. Predictions of the developed enhanced MFH for various packing configurations are compared with those obtained from Finite Element Method implementing periodic boundary conditions and very good agreements are observed. It is shown that packing configuration and geometrical specifications of short fibers can significantly affect the effective properties of the SFRC.

Keywords: Short fiber reinforced composites; Modified Eshelby tensors; Enhanced mean-field homogenization; Effective elastic properties; Analytical modelling; Finite element analysis

1. Introduction

Nowadays, short fiber reinforced composites (SFRCs) are implemented in a large number of industrial applications. These cost-effective composites have high strength-to-weight ratio and can be produced by fast and cheap processes in large series. SFRCs have become potential replacements for metallic semi-structural parts in automotive industry. For most industrial applications, estimating the effective mechanical response of SFRCs is an important engineering

[*]Corresponding author, Tel: +32470178318, E-mail: Ehsan.rashidinejad@ugent.be, Postal address: Technologiepark 46, 9052 Zwijnaarde, Ghent, Belgium.

requirement that has been studied for many years, Nomura and Chou (1984); Tucker III and Liang (1999); Karsli and Aytac (2013).

Various characteristics of SFRCs have influence on their effective properties which have been investigated in many studies. For example, by using Maxwell's far-field methodology, McCartney and Kelly (2008) and McCartney (2010) predicted the effective properties of multi-phase composites reinforced with spherical and aligned transversely isotropic spheroidal inclusions and demonstrated the effects of volume fraction of reinforcements upon the effective properties of composites. Fu et al. (2000) examined the tensile behavior of various aligned Glass and Carbon SFRCs and showed the combined effects of fiber volume fraction, average fiber length, and fiber/matrix stiffness contrast on the elastic axial modulus of SFRCs. The effects of fiber length and volume fraction on thermo-elastic properties of Carbon SFRCs were investigated in Karsli and Aytac (2013) where it was shown that increasing Carbon fiber content increases tensile strength of the composite but decreases the final strain. It should be noted that in SFRCs prepared by extrusion compounding and injection molding process, increasing volume/weight fraction of short fibers and processing rate result in decreasing the average fiber length due to fiber breakage during the process, Molnár et al. (1999); Fu et al. (2000); Karsli and Aytac (2013). For accurate prediction of the effective elastic properties of SFRCs, the main influential parameters are: 1) realistic field interactions in fibers and matrix, 2) geometrical specifications of the fibers (e.g., their exact shape, diameter, and length), and 3) packing configuration of the fibers. The latter is an important characteristic of SFRCs deserving particular attention. From experimental investigations, it is evident that short fibers may have different side-/tip- distances (i.e., distinct packing configuration), Sato et al. (1991); Arif et al. (2014).

The effective properties of SFRCs can be estimated by mean field homogenization (MFH) schemes or full-field methods. MFH schemes such as the well-known Mori-Tanaka (MT) approach (Mori and Tanaka (1973); Benveniste (1987)) are computationally efficient since they only deal with volume fraction and aspect ratio of the fibers based on simple field averaging and classical Eshelby tensors Eshelby (1957). However, only two parameters, namely volume fraction and aspect ratio, of the short fibers are clearly not enough for taking into account the distinct configuration and interactions between the closely spaced short fibers. In addition, MFHs depend only on the fundamental Eshelby solution for a single ellipsoidal inclusion (Eshelby (1957)) and thus, can neither treat the realistic cylindrical geometry of the short fibers nor their distinct packing configurations. In contrast, full-field methods such as analytical full-field approaches (e.g., Shodja and Roumi (2005); Shodja and Rashidinejad (2014)) and Finite Element Methods (FEMs) (e.g., Jain et al. (2013); Gusev (2016); Naili et al. (2020)) can accurately take into account all the interactions between the short fibers and provide accurate estimations for the effective properties of SFRCs. However, full-field approaches have to deal with intricate mathematical manipulations and high computational costs.

The main purpose of the current work is accurate and fast prediction of the effective properties of SFRCs with various fiber volume fractions incorporating realistic cylindrical geometry of the short fibers as well as their exact packing configuration. The concept of periodic microstructure approach which has been developed by Nemat-Nasser et al. (Nemat-Nasser and Taya (1981); Nemat-Nasser et al. (1982); Nemat-Nasser and Hori (2013)) and used by other researchers (e.g., Khezrzadeh (2017)) is utilized in the present study for accurate analytical modeling of closely spaced short fibers within a multi-fiber periodic representative volume element (RVE). New modified Eshelby tensors corresponding to highly interacting aligned short fibers in a multi-fiber RVE are introduced where the non-uniform variations of the homogenizing eigenstrains within the interacting short fibers are taken into account in the proposed enhanced MFH. The developed model remedies the mentioned limitations of the classical MFH methods, but preserves their advantages in terms of computational efficiency and ease-of-use. The current modified Eshelby tensors and the associated enhanced MFH approach account for cylindrical geometry of the short fibers and their realistic interactions. The effects of different packing configurations of short fibers within the multi-fiber RVE are captured as well. Moreover, finite element (FE) simulations are performed to verify the competency of the proposed method for accurate prediction of the effective properties of SFRCs. The present study is mainly concerned with accurate prediction of the effective elastic moduli of unidirectional SFRCs. However, if the short fibers have misaligned distribution, orientational averaging can be applied to the present MFH enhanced by modified Eshelby tensors (in a similar manner as in the classical MFHs, see e.g. Pettermann et al. (1997)); therefore, the effective behavior of SFRCs with misaligned fibers can also be predicted using the developed method. For demonstrating the capabilities of the proposed analytical MFH approach, the effective properties of aligned Glass and Carbon SFRCs with various configurations, volume fractions and aspect ratios are predicted. Moreover, these predictions are validated by results of FE simulations and compared with MT predictions. The effects of packing configuration of the short fibers in both single-fiber and multi-fiber models are also studied and discussed.

The current paper is organized as follows. In Section 2, the theoretical formulations associated with general multi-fiber periodic RVE are presented. The newly introduced modified Eshelby tensors corresponding to the multi-fiber RVE as well as the associated enhanced MFH are developed in Section 3. Section 4 is devoted to comprehensive examination of the effective properties of Glass and Carbon SFRCs composed of aligned cylindrical short fibers with various possible packing configurations and results of the introduced enhanced MFH are validated with precise FE simulations as well as available data in the literature and also compared with classical MT estimations. Finally, concluding remarks are presented in Section 5.

2. SFRCs with periodic multi-fiber RVE

Consider a three-dimensional (3D) anisotropic matrix with elastic moduli tensor $\boldsymbol{C}^m$ in which interacting anisotropic short fibers with elastic moduli tensor $\boldsymbol{C}^f$ are embedded. High interactions between the fibers may arise from their moderate/high volume fraction, large stiffness contrast, and large aspect ratios. The SFRC under consideration can be constructed by a 3D periodic RVE including any arbitrary number of highly interacting short fibers. The volume of the multi-fiber cubic RVE is denoted by V_0 and its dimensions in x_1-, x_2-, and x_3-directions are considered as $2L_1$, $2L_2$, and $2L_3$, respectively so that $V_0 = 8L_1L_2L_3$ (Fig. 1). Moreover, assume that Ω_i, $i = 1,2,\cdots,K$ denotes the volume of each of the K short fibers fully or partially embedded within the RVE. The fibers' domain within the multi-fiber RVE is defined by $\Omega = \bigcup_{i=1}^{K} \Omega_i$ so that clearly, the volume fraction of the short fibers is given by $v_f = \Omega/V_0$.

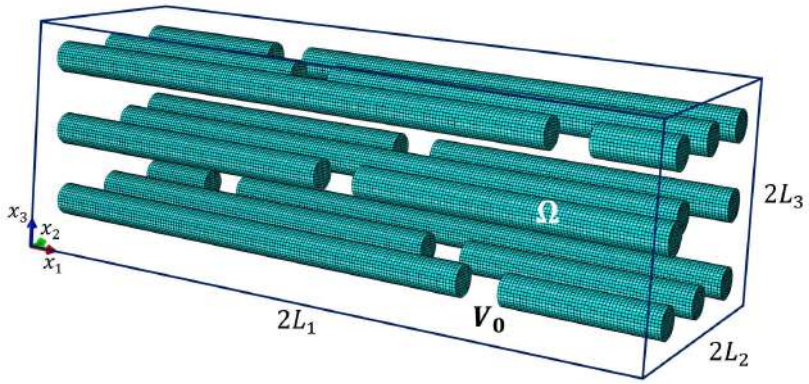

Fig. 1. Multi-fiber cubic RVE with volume V_0 and short fiber volume fraction $v_f = \Omega/V_0$ demonstrating mesh details in FE simulation.

When the composite body is subjected to a far-field strain $\boldsymbol{\epsilon}^0$ and the corresponding far-field stress $\boldsymbol{\sigma}^0$, the homogeneous strain, stress, and displacement fields will be perturbed due to the presence, as well as interactions of the short fibers. Therefore, the constitutive relations associated to each phase of the so-called multi-fiber composite RVE can be expressed as

$$\boldsymbol{\sigma}^m(\boldsymbol{x}) = \boldsymbol{C}^m\big(\boldsymbol{\epsilon}^0 + \boldsymbol{\epsilon}^d(\boldsymbol{x})\big), \quad \boldsymbol{x} \in V_0 - \Omega, \tag{1}$$

$$\boldsymbol{\sigma}^{f_i}(\boldsymbol{x}) = \boldsymbol{C}^f\big(\boldsymbol{\epsilon}^0 + \boldsymbol{\epsilon}^d(\boldsymbol{x})\big), \quad \boldsymbol{x} \in \Omega_i,\ i = 1,2,\cdots,K, \tag{2}$$

in which $\boldsymbol{\sigma}^{\mathrm{m}}(\boldsymbol{x})$ and $\boldsymbol{\sigma}^{f_i}(\boldsymbol{x})$ are the stress fields at point $\boldsymbol{x}$ located at the matrix region $V_0 - \Omega$, and each fiber's domain Ω_i, $i = 1,2,\cdots,K$, respectively and $\boldsymbol{\epsilon}^d(\boldsymbol{x})$ is the strain fluctuation (disturbance strain) at any point $\boldsymbol{x}$ in the RVE due to the presence of interacting short fibers. The strain fluctuation $\boldsymbol{\epsilon}^d(\boldsymbol{x})$ can be written in terms of the derivatives of the displacement field $\boldsymbol{u}$ (the displacement fluctuation caused by interacting short fibers) as follows

$$\epsilon^d_{kl}(\boldsymbol{x}) = \frac{1}{2}\Big(u_{k,l}(\boldsymbol{x}) + u_{l,k}(\boldsymbol{x})\Big), \quad k,l = 1,2,3. \tag{3}$$

Following the well-known equivalent inclusion concept and eigenstrain theory (Eshelby (1957); Mura (2013)), the original non-homogeneous multi-fiber RVE can be replaced by a homogeneous matrix (with elastic moduli tensor $\boldsymbol{C}^m$ everywhere) in which, over the fibers' domain Ω, proper homogenizing eigenstrains are prescribed. Thus, equivalency

of the original non-homogeneous multi-fiber RVE and its equivalent homogeneous problem including the so-called homogenizing eigenstrains requires the consistency of the stress field at any point $\boldsymbol{x} \in \Omega_i$, $i = 1,2,\cdots,K$ in the two problems. This implies that

$$\boldsymbol{\sigma}^{f\,i}(\boldsymbol{x}) = \boldsymbol{C}^f\big(\boldsymbol{\epsilon}^0 + \boldsymbol{\epsilon}^d(\boldsymbol{x})\big) = \boldsymbol{C}^m\big(\boldsymbol{\epsilon}^0 + \boldsymbol{\epsilon}^d(\boldsymbol{x}) - \boldsymbol{\epsilon}^*(\boldsymbol{x})\big), \qquad \forall \boldsymbol{x} \in \Omega_i,\ i = 1,2,\cdots,K, \tag{4}$$

where $\boldsymbol{\epsilon}^*(\boldsymbol{x})$, $\boldsymbol{x} \in \Omega$ denotes the unknown homogenizing eigenstrains prescribed over the fibers' domain.

The displacement and homogenizing eigenstrain fields satisfy the following equilibrium equations at any point $\boldsymbol{x} \in V_0$:

$$\sigma_{ij,j} = C^m_{ijkl}\big(u_{k,lj} - \epsilon^*_{kl,j}\big) = 0, \qquad i,j,k,l = 1,2,3. \tag{5}$$

As explained in Appendix A, by using Fourier representation of the periodic displacement and unknown homogenizing eigenstrain fields, the set of equilibrium equations (5) can be solved for the Fourier coefficients of the displacement field in terms of yet unknown homogenizing eigenstrain Fourier coefficients.

By substituting Eq. (A.7) into Eq. (3), the strain fluctuation $\boldsymbol{\epsilon}^d(\boldsymbol{x})$ at any point $\boldsymbol{x} \in V_0$ can be obtained as

$$\epsilon^d_{ij}(\boldsymbol{x}) = \sum_{\boldsymbol{\xi}} M_{ijmn}(\boldsymbol{\xi})\, \bar{\epsilon}^*_{mn}(\boldsymbol{\xi})\, \exp(\mathrm{i}\boldsymbol{\xi}.\boldsymbol{x}), \tag{6}$$

where

$$M_{ijmn}(\boldsymbol{\xi}) = \frac{1}{2}\big[C^m_{klmn}\xi_l\xi_j N_{ik}(\boldsymbol{\xi}) + C^m_{klmn}\xi_l\xi_i N_{jk}(\boldsymbol{\xi})\big]D^{-1}(\boldsymbol{\xi}), \tag{7}$$

and $\boldsymbol{N}(\boldsymbol{\xi})$ and $D(\boldsymbol{\xi})$ are the cofactor and determinant of the matrix $Q_{ik}(\boldsymbol{\xi}) = C^m_{ijkl}\xi_j\xi_l$ depending on the material constants of the matrix and the dimensions of the RVE in different directions (see Appendix A). Therefore, the homogenizing eigenstrain is the only field that is still unknown. Determination of the homogenizing eigenstrain field enables the calculation of the strain fluctuation and the stress field via Eqs. (6) and (1)-(2), respectively.

The unknown homogenizing eigenstrain field can be determined by using different methodologies such as full-field approaches (e.g., see Shodja and Rashidinejad (2014)). However, an accurate full-field solution may not be computationally efficient enough for engineering purposes. It is much more efficient to establish an enhanced MFH scheme based on the aforementioned theoretical framework for accurate prediction of the effective properties of SFRCs. The analytical formulations presented in Section 2 will be employed in the next section to develop novel modified Eshelby tensors corresponding to the average fields resulting in an enhanced MFH scheme. The introduced modified Eshelby tensors account for realistic interactions between the short fibers and therefore provide more realistic predictions for the effective properties of SFRCs when comparing with classical MFHs such as the well-known MT estimate.

3. Novel modified Eshelby tensors and associated enhanced MFH

In the framework of the current enhanced MFH, the multi-fiber RVE may involve any arbitrary number of short fibers while interactions between the short fibers with any packing configuration are taken into account. Moreover, the short

fibers should not necessarily have same lengths, aspect ratios, or even same geometries and each fiber can generally have distinct geometrical specifications. The average strain over the multi-fiber RVE can be written in the form

$$\langle \boldsymbol{\epsilon} \rangle_{V_0} = \boldsymbol{\epsilon}^0 = (1 - v_f)\langle \boldsymbol{\epsilon} \rangle_{V_0 - \Omega} + v_f \langle \boldsymbol{\epsilon} \rangle_{\Omega}, \tag{8}$$

in which $\langle \blacksquare \rangle_{\boldsymbol{\Gamma}} = \frac{1}{\boldsymbol{\Gamma}} \int_{\boldsymbol{\Gamma}} \blacksquare \, \mathrm{d}\boldsymbol{\Gamma}$ denotes the average of the quantity $\blacksquare$ over the region Γ. Following the well-known MFH formulation, the effective elastic moduli tensor of the SFRC can be estimated by using the strain concentration tensor $\mathbf{A}^f$ corresponding to the whole short fiber domain Ω as

$$\boldsymbol{C}^* = \boldsymbol{C}^m + v_f(\boldsymbol{C}^f - \boldsymbol{C}^m)\mathbf{A}^f. \tag{9}$$

Thus, for accurate prediction of the effective elastic moduli tensor of SFRCs, precise determination of the strain concentration tensor $\mathbf{A}^f$ incorporating the realistic interactions and geometrical specifications of the short fibers would be sufficient. For obtaining the unknown tensor $\mathbf{A}^f$, associated with each of the short fibers Ω_i, $i = 1,2,\cdots,K$, a distinct homogenizing eigenstrain distribution $\epsilon_{mn}^{*(i)}(\boldsymbol{x}) = H_{mn}^{(i)} f^{(m,n;i)}(\boldsymbol{x})$ will be considered where $f^{(m,n;i)}(\boldsymbol{x})$ denotes the variation of the yet unknown homogenizing eigenstrain component $\epsilon_{mn}^{*(i)}(\boldsymbol{x})$ with respect to the position vector $\boldsymbol{x}$ inside Ω_i, and $H_{mn}^{(i)}$ is the unknown constant coefficient of the homogenizing eigenstrain component in Ω_i. By substituting the homogenizing eigenstrains into Eq. (A.4), the corresponding Fourier coefficients associated with the multi-fiber RVE can be expressed as

$$\bar{\boldsymbol{\epsilon}}_{mn}^*(\boldsymbol{\xi}) = \sum_{i=1}^{K} v_{f_i} H_{mn}^{(i)} \langle f^{(m,n;i)}(\boldsymbol{x}) \exp(-\mathrm{i}\boldsymbol{\xi}.\boldsymbol{x}) \rangle_{\Omega_i}, \tag{10}$$

where $v_{f_i} = \Omega_i / V_0$ is the volume fraction of the i^{th} short fiber which may be fully or partially embedded within the multi-fiber RVE. Therefore, substitution of Eq. (10) into Eq. (6) results in the average strain fluctuation over each individual short fiber as

$$\langle \epsilon_{kl}^d(\boldsymbol{x}) \rangle_{\Omega_q} = \sum_{i=1}^{K} \mathcal{S}_{klmn}^{(q;i)} \langle \epsilon_{mn}^{*(i)}(\boldsymbol{x}) \rangle_{\Omega_i}, \quad q = 1,2,\cdots,K, \tag{11}$$

in which

$$\mathcal{S}_{klmn}^{(q;i)} = v_{f_i} \sum_{\boldsymbol{\xi}} M_{klmn}(\boldsymbol{\xi}) \frac{\langle f^{(m,n;i)}(\boldsymbol{x}) \exp(-\mathrm{i}\boldsymbol{\xi}.\boldsymbol{x}) \rangle_{\Omega_i}}{\langle f^{(m,n;i)}(\boldsymbol{x}) \rangle_{\Omega_i}} \langle \exp(\mathrm{i}\boldsymbol{\xi}.\boldsymbol{x}) \rangle_{\Omega_q}, \quad i,q = 1,2,\cdots,K. \tag{12}$$

$\boldsymbol{\mathcal{S}}^{(q;i)}$, $i,q = 1,2,\cdots,K$ are introduced as the novel modified Eshelby tensors which represent the average strain fluctuations over the short fiber Ω_q due to the average homogenizing eigenstrains prescribed over the short fiber Ω_i. It should be noted that classical MFH schemes (e.g., Mori and Tanaka (1973); Benveniste (1987)) deal only with uniform homogenizing eigenstrain and the corresponding interior point Eshelby tensor (Eshelby (1957); Mura (2013)) depends solely on the material properties of the matrix and aspect ratio of the ellipsoidal inclusions. In contrast, the introduced modified Eshelby tensors can incorporate the interactions between the short fibers with cylindrical geometry and thus, account for higher-order (non-uniform) distribution of the homogenizing eigenstrains over various short fibers.

Furthermore, it can be easily seen that similar to classical MFHs where the unknown constant eigenstrains do not contribute to the classical Eshelby tensor, in the current MFH the unknown constants $H_{mn}^{(i)}$ are not contributing to the modified Eshelby tensors given by Eq. (12).

For determination of the strain concentration tensor, the consistency equations for different fibers are written in the average form as

$$\boldsymbol{C}^f\left(\boldsymbol{\epsilon}^0+\langle\boldsymbol{\epsilon}^d(\boldsymbol{x})\rangle_{\Omega_q}\right)=\boldsymbol{C}^m\left(\boldsymbol{\epsilon}^0+\langle\boldsymbol{\epsilon}^d(\boldsymbol{x})\rangle_{\Omega_q}-\langle\boldsymbol{\epsilon}^*(\boldsymbol{x})\rangle_{\Omega_q}\right),\quad q=1,2,\cdots,K, \tag{13}$$

By substitution of Eq. (11) into the above set of equations and simultaneous solution for K unknown tensors $\langle\boldsymbol{\epsilon}^*(\boldsymbol{x})\rangle_{\Omega_q}$, $q=1,2,\cdots,K$, the average homogenizing eigenstrain field for each short fiber can be obtained in terms of the far-field strain $\boldsymbol{\epsilon}^0$ and can be written in the form

$$\langle\boldsymbol{\epsilon}^*(\boldsymbol{x})\rangle_{\Omega_q}=\mathfrak{A}^{(q)}\boldsymbol{\epsilon}^0,\quad q=1,2,\cdots,K, \tag{14}$$

where $\mathfrak{A}^{(q)}$ is the average eigenstrain coefficient tensor in terms of the modified Eshelby tensors, $\boldsymbol{S}^{(i;j)}, i,j=1,2,\cdots,K$. Subsequently, the strain concentration tensor of the multi-fiber RVE is obtained as

$$\mathbf{A}^f=-\frac{1}{v_f}[\boldsymbol{C}^f-\boldsymbol{C}^m]^{-1}\boldsymbol{C}^m\sum_{q=1}^{K}v_{f_q}\mathfrak{A}^{(q)}. \tag{15}$$

Now suppose that without loss of generality, the RVE contains two distinct short fiber phases Ω_1 and Ω_2 with different fiber lengths and the same material properties. This case is considered in order to investigate the competence of the developed formulation in determination of the strain concentration tensor of SFRCs with several distinct short fiber phases. By substituting the average strain fluctuation of each short fiber phase (given by Eq. (11)) into the consistency equations (13), after some manipulations it can be shown that

$$\begin{aligned}\langle\boldsymbol{\epsilon}^*(\boldsymbol{x})\rangle_{\Omega_1}&=\mathfrak{A}^{(1)}\boldsymbol{\epsilon}^0,\\ \langle\boldsymbol{\epsilon}^*(\boldsymbol{x})\rangle_{\Omega_2}&=\mathfrak{A}^{(2)}\boldsymbol{\epsilon}^0,\end{aligned} \tag{16}$$

with

$$\begin{aligned}\mathfrak{A}^{(1)}=&-\Big[\left(\boldsymbol{S}^{(1;1)}+[\boldsymbol{C}^f-\boldsymbol{C}^m]^{-1}\boldsymbol{C}^m\right)-\boldsymbol{S}^{(1;2)}\left[\boldsymbol{S}^{(2;2)}+[\boldsymbol{C}^f-\boldsymbol{C}^m]^{-1}\boldsymbol{C}^m\right]^{-1}\boldsymbol{S}^{(2;1)}\Big]^{-1}\Big(\mathbf{I}-\boldsymbol{S}^{(1;2)}\Big[\boldsymbol{S}^{(2;2)}+\\ &[\boldsymbol{C}^f-\boldsymbol{C}^m]^{-1}\boldsymbol{C}^m\Big]^{-1}\Big),\\ \mathfrak{A}^{(2)}=&-\Big[\left(\boldsymbol{S}^{(2;2)}+[\boldsymbol{C}^f-\boldsymbol{C}^m]^{-1}\boldsymbol{C}^m\right)-\boldsymbol{S}^{(2;1)}\left[\boldsymbol{S}^{(1;1)}+[\boldsymbol{C}^f-\boldsymbol{C}^m]^{-1}\boldsymbol{C}^m\right]^{-1}\boldsymbol{S}^{(1;2)}\Big]^{-1}\Big(\mathbf{I}-\boldsymbol{S}^{(2;1)}\Big[\boldsymbol{S}^{(1;1)}+\\ &[\boldsymbol{C}^f-\boldsymbol{C}^m]^{-1}\boldsymbol{C}^m\Big]^{-1}\Big).\end{aligned} \tag{17}$$

Thus, the total strain concentration tensor of the fibers domain Ω becomes

$$\mathbf{A}^f=-[\boldsymbol{C}^f-\boldsymbol{C}^m]^{-1}\boldsymbol{C}^m\frac{v_{f_1}\mathfrak{A}^{(1)}+v_{f_2}\mathfrak{A}^{(2)}}{v_f}, \tag{18}$$

which results in the effective elastic moduli tensor of the SFRC as

$$\boldsymbol{C}^{*} = \boldsymbol{C}^{m}(\boldsymbol{I} - v_{f_1}\mathfrak{A}^{(1)} - v_{f_2}\mathfrak{A}^{(2)}). \tag{19}$$

If different short fibers within the multi-fiber RVE have approximately similar configurations with respect to the nearby fibers, without loss of generality the same homogenizing eigenstrains within different fibers may be considered. This simplifying assumption can be made since eigenstrain variations arise from the elastic fields variations in the composite and assuming the same form of eigenstrain for all fibers with the same material property, geometry and relatively same interactions with adjacent fibers seems to be sufficient. Validity of this assumption for multi-fiber RVEs will be examined in Section 4.2 where the predictions of the current MFH approach enhanced by modified Eshelby tensors are compared to the accurate FE analyses for various cases, showing very good agreement. Therefore, the same variation of the homogenizing eigenstrain with respect to the local coordinates inside different short fibers is assumed and denoted by $\epsilon^{*}_{mn}(\boldsymbol{x}) = H_{mn}f^{(m,n)}(\boldsymbol{x})$, $\boldsymbol{x} \in \Omega$. The average strain fluctuation over the whole fiber domain Ω can then be expressed as

$$\langle \boldsymbol{\epsilon}^{d}(\boldsymbol{x})\rangle_{\Omega} = \boldsymbol{S}^{\mathcal{M}}\langle \boldsymbol{\epsilon}^{*}(\boldsymbol{x})\rangle_{\Omega}, \tag{20}$$

in which

$$S^{\mathcal{M}}_{klmn} = v_f \sum_{\xi} M_{klmn}(\boldsymbol{\xi})\, \frac{\langle f^{(m,n)}(\boldsymbol{x})\exp(-\mathrm{i}\boldsymbol{\xi}.\boldsymbol{x})\rangle_{\Omega}}{\langle f^{(m,n)}(\boldsymbol{x})\rangle_{\Omega}}\, \langle \exp(\mathrm{i}\boldsymbol{\xi}.\boldsymbol{x})\rangle_{\Omega}, \tag{21}$$

is the modified Eshelby tensor corresponding to the multi-fiber RVE. The consistency equation of the multi-fiber RVE can be written in an average sense over the whole fiber domain Ω as

$$\boldsymbol{C}^{f}(\boldsymbol{\epsilon}^{0} + \langle \boldsymbol{\epsilon}^{d}(\boldsymbol{x})\rangle_{\Omega}) = \boldsymbol{C}^{m}(\boldsymbol{\epsilon}^{0} + \langle \boldsymbol{\epsilon}^{d}(\boldsymbol{x})\rangle_{\Omega} - \langle \boldsymbol{\epsilon}^{*}(\boldsymbol{x})\rangle_{\Omega}). \tag{22}$$

Thus, by substitution of Eq. (20) into Eq. (22), the average eigenstrain over the fiber domain Ω can be obtained as

$$\langle \boldsymbol{\epsilon}^{*}(\boldsymbol{x})\rangle_{\Omega} = \mathfrak{A}\,\boldsymbol{\epsilon}^{0}, \tag{23}$$

where

$$\mathfrak{A} = -[\boldsymbol{S}^{\mathcal{M}} + [\boldsymbol{C}^{f} - \boldsymbol{C}^{m}]^{-1}\boldsymbol{C}^{m}]^{-1}. \tag{24}$$

Therefore, the strain concentration tensor $\mathbf{A}^{f}$ associated with the multi-fiber RVE becomes

$$\mathbf{A}^{f} = -[\boldsymbol{C}^{f} - \boldsymbol{C}^{m}]^{-1}\boldsymbol{C}^{m}\,\mathfrak{A}. \tag{25}$$

Eq. (25) can also be retrieved from substitution of Eq. (17) into Eq. (18) by letting $v_{f_1} = v_f$, $v_{f_2} = 0$, $\boldsymbol{S}^{(1;1)} = \boldsymbol{S}^{\mathcal{M}}$, and $\boldsymbol{S}^{(1;2)} = \boldsymbol{S}^{(2;1)} = \boldsymbol{S}^{(2;2)} = 0$. Consequently, the effective elastic moduli tensor of the SFRC can be given by

$$\boldsymbol{C}^{*} = \boldsymbol{C}^{m}(\mathbf{I} - v_f\,\mathfrak{A}). \tag{26}$$

It should be noted that Eqs. (24)-(26) result in expressions for the strain concentration tensor and effective elastic moduli tensors similar to dilute MT MFH. However, the fundamental distinction of the current formulation and that of MT is that the current enhanced MFH incorporates the novel modified Eshelby tensors which accurately account for the interaction effects, packing configuration, and realistic cylindrical geometry of the short fibers fully or partially embedded in the multi-fiber RVE. Moreover, in the context of classical MFHs the cylindrical geometry of the fibers is approximated

by an equivalent ellipsoidal shape (with same fiber length or same fiber aspect ratio) and hence, some physical aspects of the SFRCs are neglected. Further discussion on ellipsoidal geometry approximation in classical MFHs is given in Section 4 and it will be shown that predictions of classical MT MFH may have considerable difference when the cylindrical geometry of short fibers is approximated by different choices of: (i) ellipsoidal fibers with the same lengths, or (ii) ellipsoidal fibers with the same aspect ratios.

It is worth noting that in the context of the presented enhanced MFH, one may simply assume uniform homogenizing eigenstrains within the short fibers which is a similar assumption as in classical MFHs. But, in contrast to the classical MFHs, by assuming uniform homogenizing eigenstrains the current enhanced MFH still captures the interactions, packing configuration, and cylindrical geometry of the short fibers. However, by assuming uniform eigenstrains the predicted effective properties of the SFRC will not be as precise as those predicted by using non-uniform eigenstrains. In Section 4.1, by assuming both uniform and polynomial homogenizing eigenstrains, predictions of the enhanced MFH for effective axial Young's modulus of certain SFRCs with various packing configurations are compared with the results obtained from FE simulations.

The only yet unidentified requirement of the current enhanced MFH is exact characterization of the variations of homogenizing eigenstrain components, i.e., $f^{(m,n;i)}(\boldsymbol{x})$ in Eq. (12) and $f^{(m,n)}(\boldsymbol{x})$ in Eq. (21). From Eqs. (12) and (21) it is clearly seen that any function of coordinates for different components of the homogenizing eigenstrain field within the short fibers can be considered. However, determination of proper functions for the variation of each component of the homogenizing eigenstrain field requires further consideration of strain/stress fields inside interacting fibers which will be explained in the next section.

3.1 Homogenizing eigenstrain variations within highly interacting short fibers

The current MFH enhanced by the introduced modified Eshelby tensors will result in more accurate predictions of the effective properties of SFRCs if the assumed variations of homogenizing eigenstrain components are good approximations of those obtained from the complete full-field solution. Therefore, in this section a general framework for reliable engineering approximation of the non-uniform homogenizing eigenstrain components is presented.

For rapid yet accurate prediction of the effective properties of SFRCs, variations of the homogenizing eigenstrain components can be approximated by proper non-uniform polynomial functions. The elastic field fluctuations induced by polynomial eigenstrains prescribed within inclusions have been extensively investigated in previous studies (e.g., Mura (2013); Rashidinejad and Shodja (2019, 2020)). Variations of the homogenizing eigenstrains within the inclusions highly depend on their geometry. Since the cylindrical short fibers have one axis (axial) much greater than the two others (radial and tangential), the elastic field fluctuations within short fibers have much more variations along their axial direction in

comparison with the transverse direction (i.e., along their circular cross-section). Thus, for accurate prediction of the effective properties of SFRCs, homogenizing eigenstrain components are estimated by polynomial functions along the longitudinal axis of the short fibers. The polynomial functions $f^{(m,n;i)}(\boldsymbol{x})$ or $f^{(m,n)}(\boldsymbol{x})$ used in Eqs. (12) or (21) are considered as even functions of fibers' longitudinal axis x_1 measured with respect to the center of each fiber. Determination of $f^{(m,n)}(\boldsymbol{x})$ is presented below in details as a typical example and $f^{(m,n;i)}(\boldsymbol{x})$ can also be determined by the same fashion.

The even polynomial homogenizing eigenstrains with degree $2N$, $N > 0$ used in Eq. (21) can be written as

$$\epsilon^{*}_{mn}(\boldsymbol{x}) = H_{mn} f^{(m,n)}(\boldsymbol{x}) = H_{mn}\{1 + \alpha^{(m,n)} x_1^2 + \beta^{(m,n)} x_1^4 + \cdots + \gamma^{(m,n)} x_1^{2N}\}, \quad m,n = 1,2,3, \tag{27}$$

consisting of $6(N+1)$ unknown independent constants. By inserting the above polynomial homogenizing eigenstrains in Eq. (A.4) and then using Eq. (6), the accurate strain fluctuations at any point $\boldsymbol{x}$ can be determined. To get a good estimation of the unknown constants of the homogenizing eigenstrains, it is sufficient to evaluate the strain fluctuation components at a few points along the axis of the short fibers. Therefore, by using polynomial fitting with the same degree ($2N$) as the homogenizing eigenstrains, the strain fluctuation components can be expressed in the following form:

$$\epsilon^{d(PF;2N)}_{mn}(\boldsymbol{x}) = F_{mn}\{1 + r^{(m,n)} x_1^2 + s^{(m,n)} x_1^4 + \cdots + t^{(m,n)} x_1^{2N}\}, \quad m,n = 1,2,3, \tag{28}$$

in which the $6(N+1)$ new constants F_{mn}, $r^{(m,n)}$, $s^{(m,n)}$,…, $t^{(m,n)}$ are linear functions of the $6(N+1)$ unknowns H_{mn}, $\alpha^{(m,n)}$, $\beta^{(m,n)}$,…, $\gamma^{(m,n)}$. Substituting Eqs. (27) and (28) into the consistency equations (4) results in a set of 6 independent equations each consisting of $N+1$ distinct powers of the variable x_1 (i.e., $0, 2, 4, \cdots, 2N$). For obtaining the $6(N+1)$ unknown constants H_{mn}, $\alpha^{(m,n)}$, $\beta^{(m,n)}$,…, $\gamma^{(m,n)}$, it is then required to equate the coefficients of $N+1$ different powers of x_1 in the left- and right-hand sides of the resultant set of 6 independent consistency equations.

It should be noted that for utilizing the polynomial homogenizing eigenstrains in the introduced modified Eshelby tensors, knowledge of the ratio between coefficients of higher-degree and uniform terms (i.e., $\alpha^{(m,n)}$, $\beta^{(m,n)}$,…, $\gamma^{(m,n)}$) is sufficient. It has been realized that even by second-degree polynomial eigenstrain, the enhanced MFH accurately predicts the effective properties of SFRCs with various volume fractions, aspect ratios, and packing configurations.

4. Results and discussion

In this section, the presented modified Eshelby tensors with enhanced MFH are utilized for prediction of the effective properties of aligned Glass and Carbon SFRCs. The effects of various parameters such as fibers' packing configuration, volume fraction, aspect ratio, and fiber/matrix stiffness contrast are studied. In Section 4.1, the effective properties of aligned SFRCs based on a periodic RVE model with a single short fiber are evaluated using the current modified Eshelby tensors and enhanced MFH approach. The aim of considering the single-fiber model is examination of the accuracy of the current analytical approach compared to exact FE simulations whilst second-degree homogenizing eigenstrains are

used and no additional assumption over the homogenizing eigenstrains are considered. In addition, in studying the single-fiber model by assuming different packing configurations with too small and too large tip distances of the fibers, predictions of the presented analytical approach can be validated for limiting cases of continuous fiber composite and composite behaving close to pure matrix, respectively. Section 4.2 is devoted to the multi-fiber RVE model to further investigate the capability of the introduced modified Eshelby tensors and the associated enhanced MFH for accurate prediction of the effective properties of highly interacting SFRCs. In this section, the effective properties predicted by the assumed multi-fiber RVE are compared and validated by those available in the literature for a Polyamide/Glass SFRC. Furthermore, in Section 4.2 the remarkable effects of packing configuration and aspect ratio of the short fibers on the effective properties of Glass and Carbon SFRCs are investigated and discussed.

In order to assess the validity of the developed model, FE simulations are performed to extract the effective elastic constants of both single- and multi- fiber RVEs. It is assumed that the fibers are fully bonded with the matrix and there is no damage in the RVEs. Also, the 8-node brick elements with full integration scheme (C3D8 element in Abaqus) have been utilized to mesh the SFRCs. To capture the mechanical characteristics of the RVEs, a very fine mesh has been adopted to accurately determine the macroscopic properties. In Fig. 1, a sample of mesh details for multi-fiber RVEs is demonstrated. The periodic boundary conditions (PBCs) have been implemented on the RVEs to obtain the in-plane and out-of-plane effective properties of SFRCs. To this end, the nodal displacements at the opposite boundaries of the RVE are linked using the following equation:

$$u_j^{i+} - u_j^{i-} = 2\varepsilon_{ij}L_i, \qquad i,j = 1,2,3, \text{ (no sum on } i) \tag{29}$$

where ε_{ij} refers to the macro-strain components which are obtained from the nodal displacements u in the opposite boundaries (+ and -). Using the reference nodes, six degrees of freedom are considered for the RVEs to apply different loading conditions. It is worth mentioning that it is possible to implement the PBCs in Abaqus finite element software via *EQUATION command. More details about PBCs can be found in Garoz et al. (2019) and Ahmadi et al. (2020).

To study the effects of stiffness contrast, Glass and Carbon short fibers are considered as two typical reinforcing short fibers. For Glass fibers, the SFRC is composed of isotropic Polyamide matrix with Young's modulus $E^m = 2.1$ GPa and Poisson's ratio $\nu^m = 0.3$ reinforced with isotropic short Glass fibers with material constants $E^f = 72$ GPa and $\nu^f = 0.22$ (Wu et al. (2013)). For Carbon fibers, the SFRC is composed of the same Polyamide matrix but reinforced with *transversely isotropic* short Carbon fibers with axial Young's modulus $E_1^f = 230$ GPa, transverse Young's modulus $E_2^f = 15$ GPa, axial Poisson's ratio $\nu_{12}^f = 0.256$, transverse Poisson's ratio $\nu_{23}^f = 0.20$, axial shear modulus $G_{12}^f = 24$ GPa, and transverse shear modulus $G_{23}^f = 6.25$ GPa (Soden et al. (2004); Wu et al. (2015)). For both of the cylindrical Glass and Carbon short fibers, the fiber diameter (D_f) is assumed to be D_f =10 μm while their lengths are variable; by taking the same diameter for Glass and Carbon fibers, the effects of fiber/matrix stiffness contrast and fibers' aspect ratio

can be studied simultaneously. Two fiber volume fractions 13% and 31% are investigated which correspond to approximate mass fractions of 25% and 50% for Glass fibers and 20% and 43% for Carbon fibers, respectively. Additionally, the results obtained from the current enhanced MFH and FE analyses are compared to the effective properties estimated by classical MT MFH (Benveniste (1987)).

4.1 Single short fiber model with different configurations of interacting cylindrical fibers

In this section, the SFRC is constructed by a single-fiber periodic RVE with different configurations. The single-fiber model is studied prior to the more complicated multi-fiber RVE in order to assess the accuracy of the developed analytical method with second-degree homogenization in capturing the effects of volume fraction, packing configuration and cylindrical geometry of the fibers by detailed comparison with FE results. In the single-fiber model, no additional assumption over the homogenizing eigenstrains are imposed and therefore, studying the single-fiber model can justify the developed analytical framework. Furthermore, the limiting cases of continuous fiber composite as well as composite response approaching pure matrix behavior can also be achieved from the single-fiber model. As shown schematically in Fig. 2, the short fibers with length of $2a_1$ may be packed with different configurations while having the same volume fraction. Different packing configurations of short fibers result in distinct effective behavior of the SFRC. Suppose that w_{tip} indicates the tip-to-tip distance between the short fibers while the side-by-side distance of the fibers is represented by w_{side} (Fig. 2). The effects of packing configuration of the short fibers are also studied thoroughly in this section by considering variable tip-to-side distance ratio (w_{tip}/w_{side}) of the short fibers having the same volume fraction.

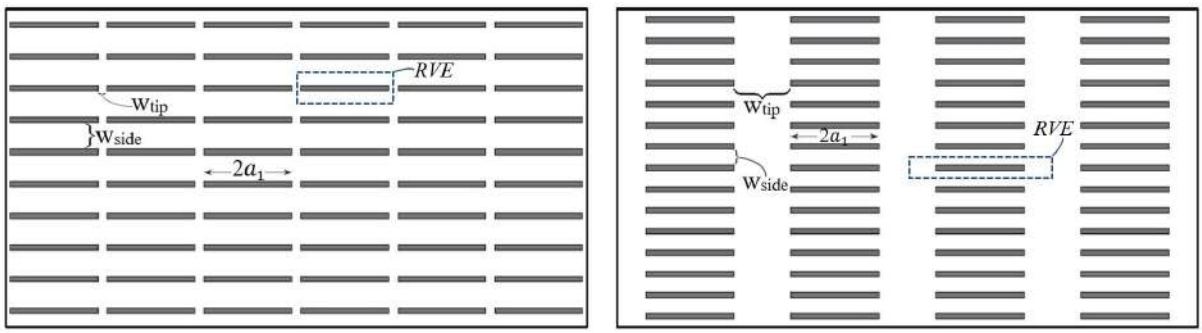

(a) (b)

Fig. 2. Two possible periodic configurations of single short fiber model for highly interacting SFRCs with (a) small tip-distance, and (b) large tip-distance of the short fibers; different packing configurations of short fibers (with same length and volume fraction) result in significant changes in the effective properties of SFRC due to the configuration effects on degree of interactions between the short fibers.

Cylindrical short fibers with aspect ratio of 20 (length of 200 μm) are examined in this section. In the context of the current MFH enhanced by modified Eshelby tensors, the homogenizing eigenstrains associated with the single-fiber model can be approximated by uniform eigenstrains or any higher-degree polynomial functions (see Section 3.1). The former is referred to as “uniform homogenization” while the latter is referred by the degree of the considered polynomial function. It is worth noting that even by using uniform homogenization within the current MFH scheme, the effects of

realistic geometry, interactions, and packing configuration of the short fibers can be taken into account. However, as it will be shown in the following, for accurate prediction of the effective properties of SFRCs non-uniform variations of the homogenizing eigenstrains should be considered in the modified Eshelby tensors and enhanced MFH approach.

For cylindrical short fibers with length of $2a_1$ (a_1=100 μm for fibers with aspect ratio of 20), the homogenizing eigenstrain components with second-degree polynomial variation are evaluated for the single-fiber as explained in Section 3.1. By measuring x_1 from the center of the short fibers, the normal components of the second-degree polynomial homogenizing eigenstrain field are considered in the form

$$\epsilon^*_{mn}(\boldsymbol{x}) = H_{mn}\left(1 + \alpha^{sf}\left(\frac{x_1}{a_1}\right)^2\right), \quad m = n, \tag{30}$$

while the shear homogenizing eigenstrain components are still constant. For the single-fiber model with arbitrary configuration, the associated average function $\langle(1 + \alpha^{sf}(x_1/a_1)^2)\exp(-\mathrm{i}\boldsymbol{\xi}.\boldsymbol{x})\rangle_\Omega$ required for determination of the modified Eshelby tensor in Eq. (21) is given in Appendix B. Calculated values of the constant α^{sf} obtained for different fiber volume fractions and fiber types are provided in Table 1. It is clear that for each configuration of fibers with distinct tip-to-side distance ratio (w_{tip}/w_{side}), coefficient of the second-degree term would be different. While in each certain case the coefficient α^{sf} for Carbon fibers is generally larger than that for Glass fibers, the values of α^{sf} for v_f=31% are smaller in comparison with the same case in v_f=13%.

Table 1. Values of the constant α^{sf} corresponding to second-degree polynomial homogenizing eigenstrain field (Eq. (30)) obtained for two different volume fractions and various tip-to-side distance ratios of Glass and Carbon short fibers.

	α^{sf}			
	v_f=13%		v_f=31%	
w_{tip}/w_{side}	Carbon fiber	Glass fiber	Carbon fiber	Glass fiber
0.25	-0.47	-0.44	-0.15	-0.15
0.5	-0.62	-0.59	-0.31	-0.29
1	-0.68	-0.65	-0.45	-0.43
4	-0.65	-0.62	-0.49	-0.47
10	-0.58	-0.56	-0.44	-0.42

Convergence of the current model is examined for both Glass and Carbon SFRCs with two different fiber volume fractions of 13% and 31%. For Glass and Carbon SFRCs with equal tip-to-tip and side-by-side distance of the short fibers, the effective axial Young's moduli predicted by the presented enhanced MFH for various upper/lower limits of the series in Eq. (21) are demonstrated in Fig. 3(a). In addition, the computational times (in seconds) required for evaluation of the effective elastic moduli tensor of the SFRCs are indicated in Fig. 3(a) for each of the series limits. The indicated computational times correspond to calculation of the modified Eshelby tensors and effective moduli tensor on only one

core processor of Core i7 CPU and 16 GB of memory, while FE analysis on the same CPU with 4 parallel core processors and 16 GB of memory takes 634 seconds; this comparison clearly demonstrates the computational efficiency of the present enhanced MFH compared to FE analysis. The results provided in Fig. 3(a) show that the developed MFH enhanced by modified Eshelby tensors benefits from the significant advantages of fast convergence of Fourier series solution and computational efficiency of MFH approaches. Fig. 3(b) demonstrates the predicted effective Young's moduli of Carbon SFRCs with volume fractions of 13% and 31% for different packing configurations of the fibers (different tip-to-side distance ratio w_{tip}/w_{side} in logarithmic scale). FE accurate results as well as variations of the predicted axial Young's moduli using both uniform and second-degree polynomial homogenizations are illustrated in Fig. 3(b). Clearly, the use of second-degree polynomial homogenizing eigenstrains results in much better agreement with accurate FE results. The maximum difference between the effective Young's moduli predicted via uniform and second-degree polynomial homogenizations are 25 and 11 percent for volume fractions of 13% and 31%, respectively.

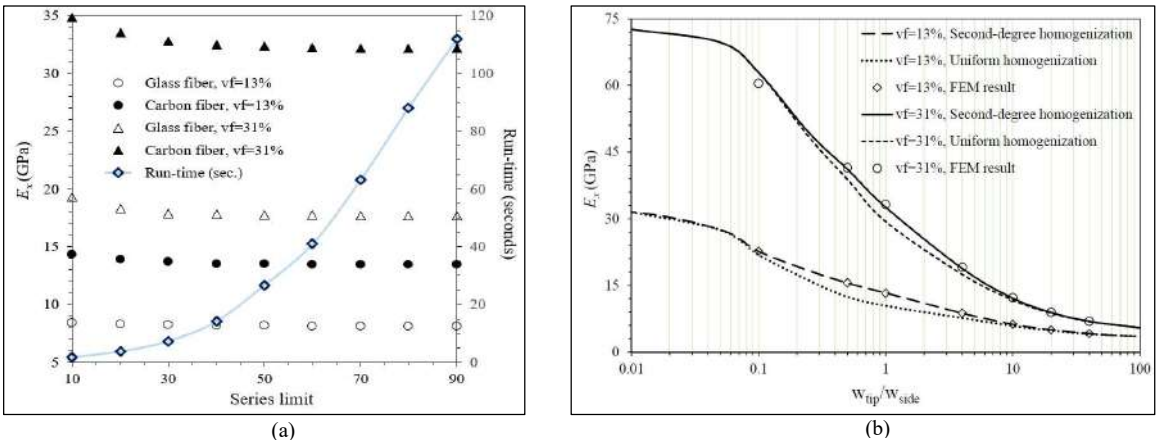

(a) (b)

Fig. 3. (a) Convergence of the predicted effective Young's modulus E_x for Glass and Carbon SFRCs with 13% and 31% volume fractions and associated calculation time (in seconds) versus different series limits, and (b) variations of the predicted effective axial Young's modulus of Carbon SFRC with 13% and 31% volume fractions evaluated by uniform and second-degree homogenization for different packing configuration (tip-to-side distance ratio) of short fibers in logarithmic scale.

In Fig. 4, variations of the predicted effective Young's modulus E_x for both Glass and Carbon SFRCs with 13% volume fraction calculated by second-degree MFH as well as those obtained from FEM simulations are illustrated. In addition, the effective Young's moduli predicted by the well-known classical MT approach (Benveniste (1987)) are also provided; these estimates are in exact agreement with the results of commercial Digimat software (Digimat (2011)). It should be noted that since classical MT MFH considers the fibers to have ellipsoidal geometry, the cylindrical short fiber may be estimated by (i) the ellipsoidal one with equal volume and the same length, or (ii) an ellipsoidal fiber with equal volume and the same aspect ratio meaning that the ellipsoidal fiber would be 14.5% longer than the cylindrical fiber. These two different ellipsoidal estimations of classical MT MFH are indicated in Fig. 4. The classical MT MFH cannot take into account different configurations of short fibers and provides the same results for different packing configurations. However, the current enhanced MFH with the modified Eshelby tensors considers the effects of packing

configuration and thus, provides accurate predictions when compared to results of refined FEM simulations. It can be seen in Fig. 4 that the difference between estimates of the current enhanced MFH and those of FEM is less than 1% for all cases. In addition, for the limiting case where $w_{tip}/w_{side}\rightarrow 0$, the effective Young's modulus predicted by the current enhanced MFH converges to that of unidirectional continuous fiber reinforced composite and therefore, this limiting case provides further validation of the present MFH approach.

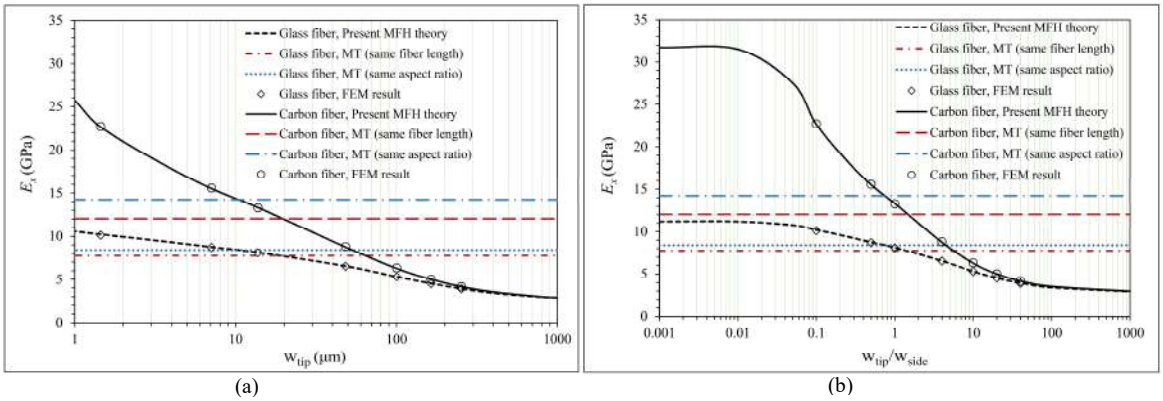

(a) (b)

Fig. 4. Variations of the effective axial Young's modulus of Glass and Carbon SFRCs with 13% volume fraction for different packing configurations of short fibers with: (a) various tip distance of fibers, and (b) various tip-to-side distance ratio in logarithmic scale.

Next, the results are shown for a much higher volume fraction, where the interaction effects are expected to be much higher. The effective axial Young's modulus E_x predicted for Glass and Carbon SFRCs with 31% volume fraction are demonstrated in Fig. 5 with respect to tip distance of fibers (Fig. 5(a)) as well as fibers' tip-to-side distance ratio (Fig. 5(b)). It is shown that when the fibers have the same side and tip distances ($w_{tip}/w_{side}=1$), the effective Young's modulus E_x is in the range between the two different classical MT estimates (i.e., ellipsoidal estimation with same fiber length or with same aspect ratio); in contrast, increasing or decreasing of fibers' tip distance result in, respectively, significant decreasing or increasing of the effective axial Young's modulus of the SFRC. For the same SFRCs, variations of the predicted transverse Young's modulus E_y versus fibers' side distance and tip-to-side distance ratio are illustrated in Figs. 5(c) and 5(d), respectively. Variations of the effective axial and transverse Poisson's ratios with respect to fibers' tip-to-side distance ratio are also plotted in Figs. 5(e) and 5(f), respectively. It is found that classical MT generally overestimates both the axial and transverse Poisson's ratio's. The effective properties of the examined SFRCs with 31% fiber volume fraction predicted by the enhanced MFH demonstrate very good agreement with the results of FEM simulations. It is worth noting that as it can be observed in Figs. 5(a)-(f), for the limiting case of $w_{tip}\rightarrow 0$ the effective properties of the Glass and Carbon SFRCs predicted by the enhanced MFH approach converge to those of continuous fiber composite with same volume fraction. Hence, these convergences demonstrate additional verification of the current enhanced MFH and reveal that the present MFH approach accurately accounts for realistic specifications and configuration of the short fibers which is not incorporated by classical MFHs.

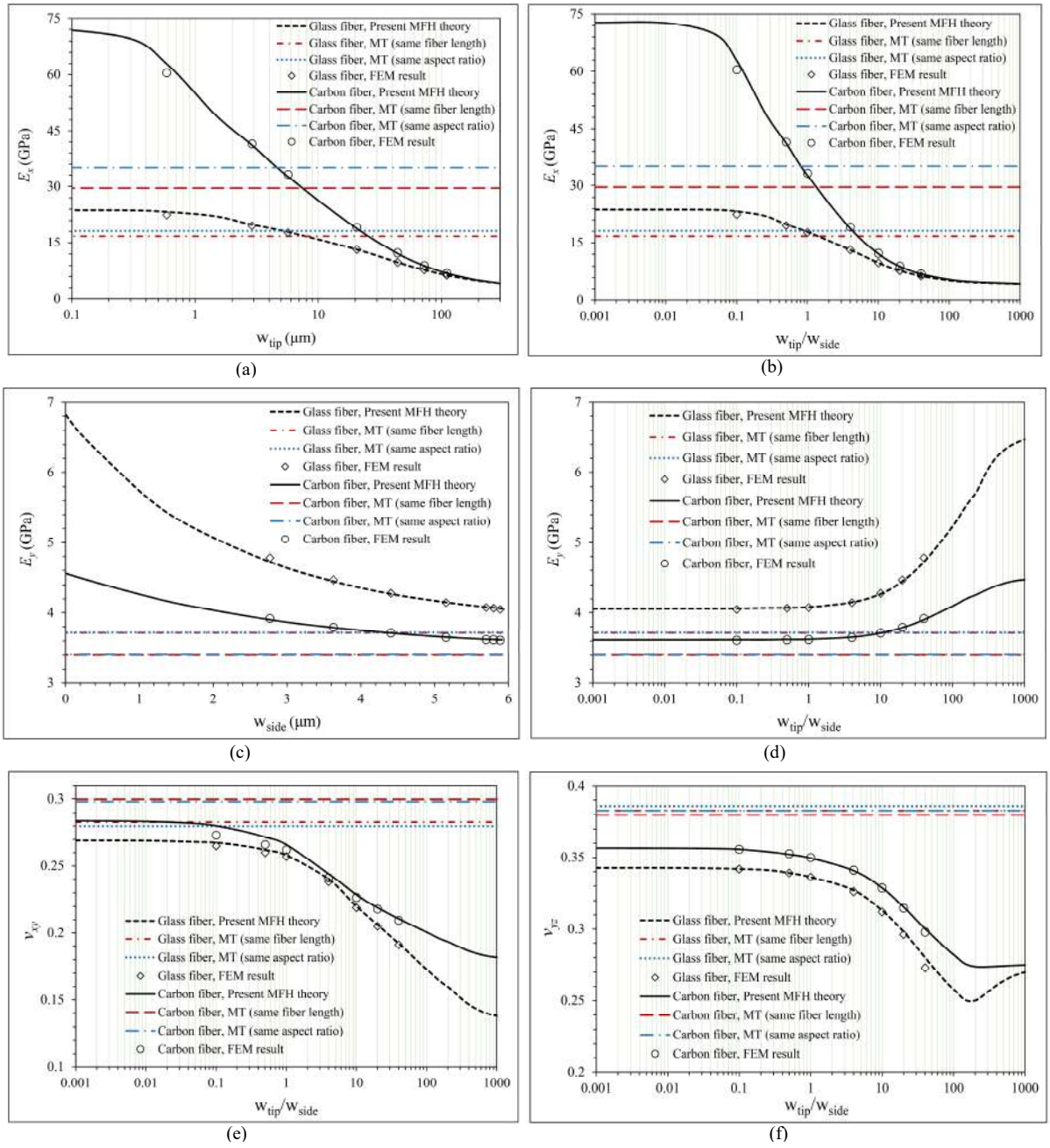

Fig. 5. Variations of the effective properties of Glass and Carbon SFRC with 31% volume fraction for different fiber packing configurations: (a) axial Young's modulus versus tip distance of fibers, (b) axial Young's modulus versus fibers' tip-to-side distance ratio, (c) transverse Young's modulus versus side distance of fibers, (d) transverse Young's modulus versus fibers' tip-to-side distance ratio, (e) axial Poisson's ratio versus fibers' tip-to-side distance ratio, and (f) transverse Poisson's ratio versus fibers' tip-to-side distance ratio.

4.2 Multi-fiber RVE model with different configurations of interacting cylindrical short fibers

In this section, the SFRC is composed of a multi-fiber periodic RVE. To this end, a multi-fiber RVE with 17 aligned short fibers is considered (see Fig. 1). While the central fiber is fully embedded within the considered RVE, the other sixteen fibers are partially embedded and have different lengths inside the RVE such that when the periodic RVE constructs the SFRC, all the fibers would have equal lengths. It can be seen in Fig. 1 that in the multi-fiber RVE, fibers in different locations have different involving lengths scattered in the RVE: two fibers with 12.5%, two with 25%, two

with 37.5%, four with 50%, two with 62.5%, two with 75%, two with 87.5%, and the central one with 100% of the length. For the multi-fiber RVE with the ascribed locations of the fibers which may have arbitrary tip/side distance (packing configuration), the normal components of the homogenizing eigenstrain are considered as second-degree polynomial of the form $\epsilon^*_{mn}(\boldsymbol{x}) = H_{mn}(1 + \alpha^{mf}(x_1/a_1)^2),\ m = n$ (with x_1 measured with respect to the center of each fiber) while the shear homogenizing eigenstrain components are considered to be uniform. Subsequently, the associated average function $\langle(1 + \alpha^{mf}(x_1/a_1)^2)\exp(-\mathrm{i}\boldsymbol{\xi}.\boldsymbol{x})\rangle_\Omega$ (average over all of the fibers within the multi-fiber RVE) required for determination of the modified Eshelby tensor in Eq. (21) is given in Appendix B. In Section 4.2.1, by applying the developed analytical method on the assumed multi-fiber RVE the predicted effective properties are compared and validated by those available in the literature for a Polyamide/Glass composite. Section 4.2.2 is devoted to studying the effects of packing configuration of the Glass and Carbon short fibers in the multi-fiber RVE by considering variable tip and side distances of the short fibers. Subsequently, the significant effects of aspect ratio of both Glass and Carbon short fibers are investigated in Section 4.2.3 and the predictions of the current enhanced MFH are verified by FE simulations and compared with those of MT MFH.

4.2.1 Comparison of the predicted effective properties with available numerical data in Mirkhalaf et al. (2020)

In this section, the developed enhanced MFH is utilized for prediction of the effective properties of aligned Polyamide/Glass composite using the introduced multi-fiber RVE and these predictions are compared with available numerical data in the literature for effective properties of the same SFRC. Mirkhalaf et al. (2020) have modeled the SFRC in finite elements by various multi-fiber RVEs as well as single-fiber model. Therefore, comparison of the effective properties predicted by the current enhanced MFH for both single-fiber and multi-fiber RVEs verifies the implementation of the present analytical approach and also validates the assumed configuration in the multi-fiber RVE. The Polyamide/Glass composite is composed of unidirectional short glass fibers with aspect ratio of 24 and volume fraction of 10%; the Young's modulus of Glass fibers and Polyamide matrix are 76 GPa and 3.1 GPa while their Poisson's ratio are 0.22 and 0.35, respectively (see Table 4 of Mirkhalaf et al. (2020)). The effective properties of the composite evaluated by four different multi-fiber RVEs (using Digimat-FE) are given in Table 1 of Mirkhalaf et al. (2020); the effective properties obtained from different RVEs do not have considerable differences and therefore, the average values are given in Table 2 below. The effective properties of the same composite are also obtained by the developed enhanced MFH for both single-fiber and multi-fiber RVEs. It should be noted that as shown in Section 4.1, the current analytical approach is more efficient than FE simulation while it provides accurate predictions for the effective properties of SFRCs. By employing the developed enhanced MFH, the effective properties of the composite are obtained for different physically possible packing configurations of w_{tip}/w_{side}=1, w_{tip}/w_{side}=4 and w_{tip}/w_{side}=10 (equivalent to tip distance of the

fibers in the range of $1.7D_f$<w_{tip}<$12.7D_f$); the latter seems more similar to the fibers' tip distances in multi-fiber RVEs considered by Mirkhalaf et al. (2020). The corresponding effective properties are listed in Table 2. It can be observed that the obtained effective properties for the considered packing configurations do not have considerable difference and are in very good agreement with those taken from Mirkhalaf et al. (2020). In addition, in Mirkhalaf et al. (2020) it is expressed that the effective properties of an aligned single-fiber model with equal side and tip distance are in good agreement with those of the aligned multi-fiber RVEs. To check this statement for the considered composite, the effective properties of the corresponding single-fiber model with w_{tip}/w_{side}=1 are calculated using the developed enhanced MFH approach and compared with those of the multi-fiber RVEs in Table 2. It can be concluded that for the considered Polyamide/Glass composite, predictions of the single-fiber model with the assumed configuration (equal side and tip distance of the fibers) are also in good agreement with those of multi-fiber models. However, in Mirkhalaf et al. (2020) the single-fiber model with equal tip and side distances is examined by FE simulation and only for one composite case (Polyamide/Glass composite with fiber aspect ratio of 24 and volume fraction of 10%) the effective properties predicted by single-fiber and multi-fiber RVEs are compered. It is worth noting that as shown in Figs. 4 and 5, the effective properties of both Glass and Carbon SFRCs obtained from the single-fiber model considerably change with the packing configuration of the short fibers while it will be shown in the next section that effective properties predicted by multi-fiber RVE do not have such variations for the packing configurations of $1<w_{tip}/w_{side}<10$. For demonstration of the considerable effects of packing configuration in the single-fiber model, the corresponding effective properties evaluated by the current enhanced MFH for w_{tip}/w_{side}=4 and w_{tip}/w_{side}=10 are also provided in Table 2. It is clear that the effective axial modulus in the single-fiber model is very sensitive to the fiber packing configuration (w_{tip}/w_{side} ratio) and hence, this parameter must be carefully determined when modeling the SFRC with the simple single-fiber. In addition, as it will be shown in the next section, for higher fiber/matrix stiffness contrast (Carbon fibers instead of Glass fibers) the effective axial modulus of the composite obtained from the multi-fiber RVE considerably differs from that of the single-fiber model with packing configuration of w_{tip}/w_{side}=1. Consequently, for calibrating a single-fiber model (as in Mirkhalaf et al. (2020)) to generate accurate predictions as the multi-fiber RVE, the fiber/matrix stiffness contrast as well as other influential parameters such as fiber volume fraction and aspect ratio should be investigated for each SFRC with distinct characteristics. Moreover, for such calibrations predicting the effective properties of the SFRC via the multi-fiber RVE is always required which can be performed through FE simulation of the multi-fiber RVE (as in Mirkhalaf et al. (2020)) or by using the presented efficient analytical approach and enhanced MFH of the multi-fiber RVE with the corresponding modified Eshelby tensors.

Table 2. Effective elastic properties of Polyamide/Glass SFRC with 10% volume fraction predicted by multi-fiber RVEs and single-fiber model.

	E_{11} (GPa)	E_{33} (GPa)	G_{13} (GPa)	ν_{13}	ν_{23}
Data from Mirkhalaf et al. (2020)	8.60	3.91	1.40	0.33	0.44
Multi-fiber RVE with w_{tip}/w_{side}=1	8.89	3.95	1.39	0.34	0.44
Multi-fiber RVE with w_{tip}/w_{side}=4	8.87	3.94	1.39	0.34	0.44
Multi-fiber RVE with w_{tip}/w_{side}=10	8.59	3.94	1.39	0.33	0.44
Single-fiber with w_{tip}/w_{side}=1	8.71	3.94	1.39	0.33	0.44
Single-fiber with w_{tip}/w_{side}=4	7.78	3.95	1.38	0.33	0.44
Single-fiber with w_{tip}/w_{side}=10	6.86	3.96	1.37	0.32	0.43

4.2.2 Effects of packing configuration of the short fibers

In this section, the significant effects of packing configuration of the short fibers within the multi-fiber RVE are studied and compared with those in the single-fiber model. As shown in Fig. 6, variations of the predicted effective axial Young's modulus of the SFRC composed of the described multi-fiber RVE with 13% fiber volume fraction and aspect ratio of 20 are demonstrated for different packing configurations of both Glass and Carbon short fibers. In addition, in Fig. 6 variations of the same effective property of the SFRCs predicted by the single-fiber model are included for both Glass and Carbon short fibers; it is shown that for Carbon fibers when the tip-to-side distance of short fibers is between 0.4 and 6, the effective Young's modulus obtained from the multi-fiber model is higher than both the Young's moduli from the single-fiber model and that of the classical MT MFH.

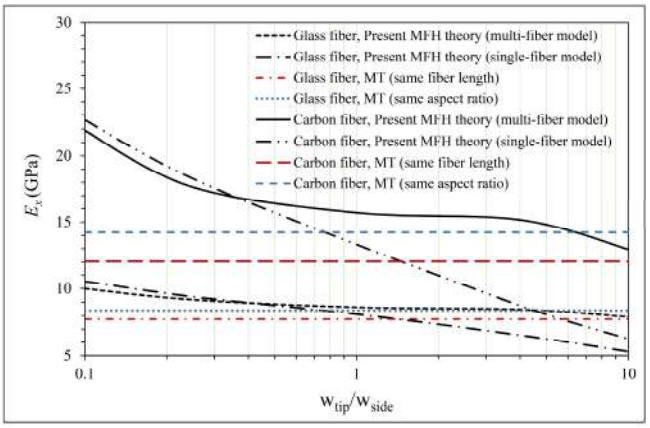

Fig. 6. Variations of the effective axial Young's modulus of Glass and Carbon SFRC with 13% volume fraction versus tip-to-side distance of short fibers in both multi-fiber and single-fiber models.

Next, the results are shown again for a much higher volume fraction, where the interaction effects are expected to be much higher. Variations of the effective axial and transverse Young's modulus of both Glass and Carbon SFRCs with volume fraction of 31% and aspect ratio of 20 (fiber length of 200 μm) for different packing configurations are illustrated in Figs. 7(a) and 7(b), respectively. Moreover, effective Young's moduli predicted by both single-fiber and multi-fiber models are demonstrated. The effective properties predicted by the current enhanced MFH incorporating modified Eshelby tensors show very good agreement with the results of FE analyses. It is realized that for both Glass and Carbon SFRCs with w_{tip}/w_{side} less than 10, the effective axial modulus of the considered RVE is greater than that estimated by classical MT MFH with either the same fiber length or the same aspect ratio of the ellipsoid approximation; for Carbon short fibers, when the fibers have almost equal side and tip distances, the effective axial Young's modulus is 32% and 20% greater than classical MT estimate with same fiber length and same aspect ratio of the ellipsoid approximations, respectively. Furthermore, for lower fiber/matrix stiffness contrast (Glass fibers), the effective axial modulus based on the considered multi-fiber RVE with $1<w_{tip}/w_{side}<10$ slightly differs from that of the single-fiber model with $w_{tip}/w_{side}=1$ while for higher fiber/matrix stiffness contrast (Carbon fibers), there is considerable difference between predictions of the multi-fiber RVE with $1<w_{tip}/w_{side}<10$ and that of the single-fiber model with $w_{tip}/w_{side}=1$. On the other hand, the effective transverse Young's modulus of Glass and Carbon SFRCs would be, respectively, around 10% and 7% higher than that estimated by classical MT MFH. The predicted effective Poisson's ratio's of the Glass and Carbon SFRCs are demonstrated in Figs. 7(c) and 7(d) where it has been shown that classical MT overestimates the axial and transverse Poisson's ratios of both Glass and Carbon SFRCs. The transverse Poisson's ratio of the assumed Glass and Carbon SFRCs is at least 12% and 7% smaller than the classical MT estimate, respectively.

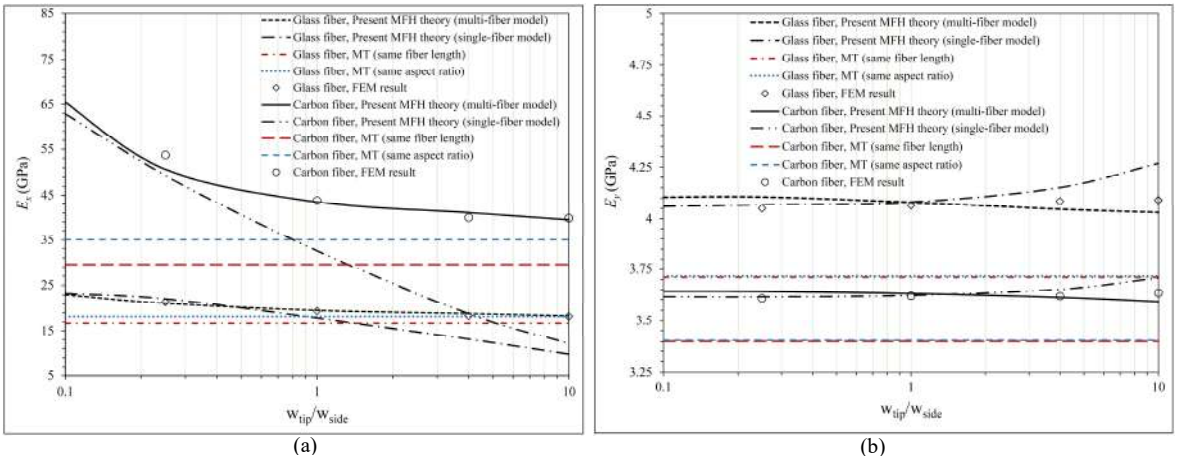

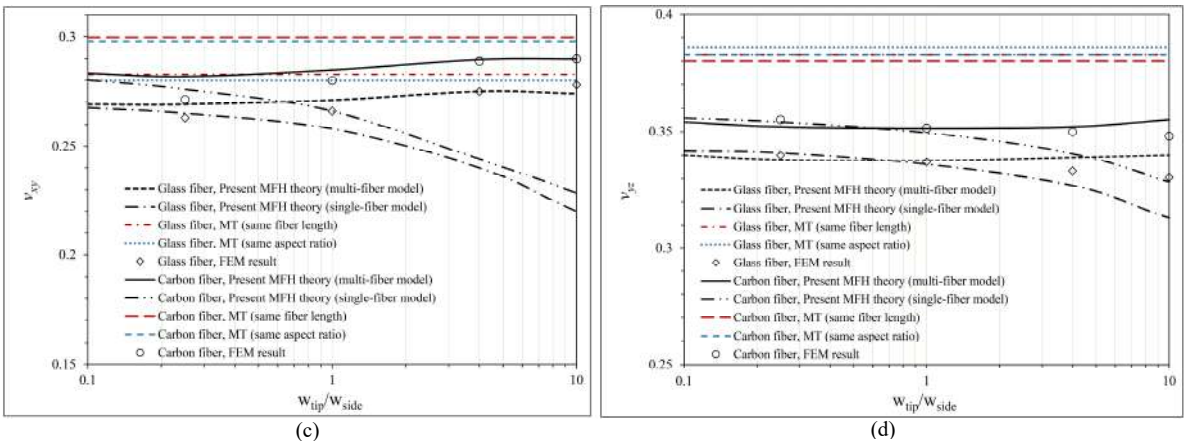

(c) (d)

Fig. 7. Variations of the effective properties of Glass and Carbon SFRC with 31% volume fraction for single- and multi-fiber models against tip-to-side distance of fibers: (a) axial Young's modulus, (b) transverse Young's modulus, (c) axial Poisson's ratio, and (d) transverse Poisson's ratio. Results of FEM simulations for several distinct cases pertinent to the multi-fiber model are provided.

4.2.3 Effects of aspect ratio of the short fibers

In order to study the effects of aspect ratio of short fibers on the effective properties of highly interacting SFRCs, the effective longitudinal Young's moduli corresponding to 31% volume fraction of both Carbon and Glass short fibers with different aspect ratios are studied by the introduced enhanced MFH with second-degree homogenization of the multi-fiber RVE as well as FE simulations. Two different configurations for the short fibers are assumed and results for both configurations are compared with those of identical FE simulations and MT predictions. In the first configuration, short fibers are considered to have equal side and tip distances (w_{tip}/w_{side}=1). In the second configuration, tip distance of the short fibers is supposed to be a relatively large value equal to $w_{tip}=6.5D_f$ for all of the examined aspect ratios; there are lack of information in the literature about fiber distancing in SFRCs and therefore, this value is only chosen as to be representative of relatively large tip distance of the fibers.

In Figs. 8(a) and 8(b), variations of the effective axial Young's modulus of, respectively, Glass and Carbon SFRCs with 31% fiber volume fraction evaluated by the current enhanced MFH for the two different configurations are illustrated and compared with estimates of the well-known MT MFH. Results of FEM simulations for the same multi-fiber models are also provided for both Glass and Carbon SFRCs in Figs. 8(a) and 8(b), respectively, and good agreement between the predictions of enhanced MFH approach using second-degree polynomial homogenization and results of FEM analyses is achieved for both Glass and Carbon SFRCs. It can be observed in Fig. 8(a) that for Glass SFRCs and packing configuration of $w_{tip}=6.5D_f$, classical MT with same aspect ratio generally overestimates the effective axial Young's modulus of the considered multi-fiber RVE and, in this configuration, classical MT with same fiber length gives better prediction of the effective axial modulus. However, for the packing configuration of $w_{tip}=w_{side}$ classical MT with same aspect ratio overestimates the effective axial modulus only for aspect ratios larger than 40 while it underestimates the effective axial modulus for aspect ratios between 20 and 40. In contrast, for Carbon short fibers with aspect ratios between

20 and 50, for both of the fiber configurations the effective axial modulus of the SFRC is larger than MT estimates. The maximum difference between the results of the enhanced higher-order MFH and MT MFH with the same fiber length occurs for the aspect ratio of 20 and is around 32% and 25% for the two configurations of $w_{tip}/w_{side}=1$ and $w_{tip}=6.5D_f$, respectively; the differences are calculated with respect to the accurate result of the enhanced MFH. For the aspect ratios larger than 60, the effective axial modulus of the Carbon SFRC lies between the two different MT estimates with the same length and same aspect ratio of the fibers. These variations reveal that for Carbon SFRCs when fiber aspect ratio is less than 60, classical MT with same aspect ratio can better predict the axial modulus of the composite while for aspect ratios more than 70, classical MT with same fiber length gives better prediction of the effective axial modulus.

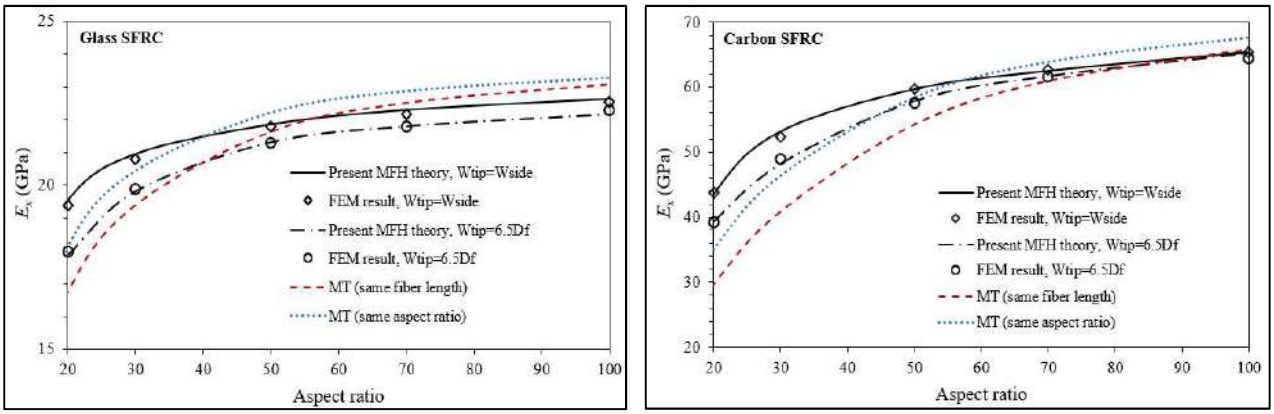

(a) (b)

Fig. 8. Variations of the effective axial modulus versus fiber aspect ratio for (a) Glass SFRC, and (b) Carbon SFRC, with 31% fiber volume fraction and different configurations of $w_{tip}/w_{side}=1$ and $w_{tip}=6.5D_f$ compared to FE results of identical models as well as classical MT predictions.

5. Conclusions

The current paper investigates the effective behavior of SFRCs reinforced with highly interacting short fibers. Novel modified Eshelby tensors and enhanced MFH associated with multi-fiber RVE are developed and utilized for accurate prediction of the effective properties of SFRCs. It is shown that the presented enhanced MFH incorporating the introduced modified Eshelby tensors remedies the limitations of classical MFH methods by taking into account the realistic characteristics of the SFRC even with highly interacting fibers while preserving the computational efficiency of MFHs. Furthermore, the exact cylindrical geometry of the fibers as well as their packing configuration are incorporated. Comparisons between the predictions of the current enhanced MFH and precise FEM simulations reveal that the developed enhanced MFH provides accurate predictions for the effective properties of SFRCs. By studying both single- and multi-fiber models for Glass and Carbon SFRCs with various volume fractions and aspect ratios, it is concluded that accurate prediction of the effective properties of SFRCs needs further attention to the fibers' configuration and that the packing configuration of short fibers as well as their interactions have significant effects on the effective properties of aligned SFRCs. It is also revealed that for accurate prediction of the effective properties of Glass and Carbon SFRCs,

non-uniform homogenizing eigenstrains (rather than uniform homogenization) should be taken into account throughout the introduced modified Eshelby tensors. In the single-fiber model, effective axial Young's modulus of aligned SFRCs with different volume fractions of 13% and 31% is highly sensitive to the side and tip distance of short fibers. It is shown that in the considered multi-fiber RVE with 31% fiber volume fraction and aspect ratio of 20, when the short fibers have equal side and tip distances, the effective axial Young's modulus of Carbon and Glass SFRCs are, respectively, 32% and 14% larger than the classical Mori-Tanaka (MT) estimate with the same fiber length of the ellipsoid approximations. It has been shown that the current enhanced MFH is computationally much more efficient than FE analysis in terms of computational time. Therefore, the introduced analytical formulation for the modified Eshelby tensors and the resulting enhanced MFH approach provide a robust theoretical framework for accurate and fast prediction of the effective elastic properties of SFRCs with any configuration/specification of short fibers which is of particular interest for various industrial applications of SFRCs. It is noted that although we have shown that geometrical specifications and packing configuration of short fibers can affect the effective elastic properties of the SFRC, they have even more effects on composite behavior beyond the elastic regimes. By increasing the load, SFRC shows a highly non-linear behavior which is mainly attributed to matrix plasticity and possible fiber matrix debondings. To deal with these inelastic scenarios, one may take the advantages of finite element solutions for multi-fiber volume elements which lead to expensive computational cost. Another approach which is largely used in practice is to modify MFH methods for matrix plasticity simply by enhancing the strain concentration tensor (mainly based on MT approach) of the matrix component. Therefore, the current work can still benefit from these modifications while it clearly has a better accuracy in comparison to the typical MFH methods.

Acknowledgements

The authors acknowledge the financial support from EIT Raw Materials project "RELICARIO" under Grant Agreement No. 18239.

The work of M. Hajikazemi forms part of the research programme of DPI, project 812T17.

Appendix A. Analytical solution for periodic inclusions with arbitrary eigenstrains

Associated with a 3D periodic multi-fiber RVE, the displacement and strain fluctuations can be expressed in terms of the following Fourier series, respectively (see Shodja and Rashidinejad (2014); Rashidinejad and Naderi (2018)):

$$u_k(\boldsymbol{x}) = \sum_{\xi} \bar{u}_k(\boldsymbol{\xi}) \exp(\mathrm{i}\boldsymbol{\xi}.\boldsymbol{x}), \tag{A.1}$$

$$\epsilon^d_{kl}(\boldsymbol{x}) = \sum_{\xi} \bar{\epsilon}^d_{kl}(\boldsymbol{\xi}) \exp(\mathrm{i}\boldsymbol{\xi}.\boldsymbol{x}), \tag{A.2}$$

where $\boldsymbol{\xi}$ is the wave vector of the given periods and $\bar{u}_k(\boldsymbol{\xi})$ and $\bar{\epsilon}^d_{kl}(\boldsymbol{\xi})$ are the Fourier coefficients corresponding to the (yet unknown) displacement and strain fluctuations. Accordingly, the solution for the homogenizing eigenstrains also takes on the Fourier series form with the same periods as

$$\epsilon^*_{kl}(\boldsymbol{x}) = \sum_{\xi} \bar{\epsilon}^*_{kl}(\boldsymbol{\xi}) \exp(\mathrm{i}\boldsymbol{\xi}.\boldsymbol{x}), \tag{A.3}$$

where

$$\bar{\epsilon}^*_{kl}(\boldsymbol{\xi}) = \frac{1}{8L_1L_2L_3} \int_{\Omega} \epsilon^*_{kl}(\boldsymbol{x}') \exp(-\mathrm{i}\boldsymbol{\xi}.\boldsymbol{x}') \, \mathrm{d}\boldsymbol{x}'. \tag{A.4}$$

Substitution of Eqs. (A.1) and (A.3) into the equilibrium equation (5) results in the following system of equations for the unknowns $\bar{u}_k$:

$$C^m_{ijkl}\xi_l\xi_j\bar{u}_k(\boldsymbol{\xi}) = -\mathrm{i}C^m_{ijkl}\xi_j\bar{\epsilon}^*_{kl}(\boldsymbol{\xi}). \tag{A.5}$$

By defining the 3×3 symmetric matrix $Q_{ik}(\boldsymbol{\xi}) = C^m_{ijkl}\xi_j\xi_l$ and solving the system of equations (A.5), the Fourier coefficients $\bar{u}_k(\boldsymbol{\xi})$ can be obtained as

$$\bar{u}_k(\boldsymbol{\xi}) = -\mathrm{i}C^m_{plmn}\xi_l\bar{\varepsilon}^*_{mn}(\boldsymbol{\xi}) \, N_{kp}(\boldsymbol{\xi})D^{-1}(\boldsymbol{\xi}), \tag{A.6}$$

where $\boldsymbol{N}(\boldsymbol{\xi})$ and $D(\boldsymbol{\xi})$ are the cofactor and determinant of the matrix $\boldsymbol{Q}(\boldsymbol{\xi})$. Consequently, by substituting (A.6) into (A.1) the displacement field is expressed in terms of the Fourier coefficients of the homogenizing eigenstrain field:

$$u_i(\boldsymbol{x}) = -\mathrm{i}\sum_{\xi} \left[C^m_{klmn}\xi_l N_{ik}(\boldsymbol{\xi})D^{-1}(\boldsymbol{\xi})\right] \bar{\varepsilon}^*_{mn}(\boldsymbol{\xi}) \exp(\mathrm{i}\boldsymbol{\xi}.\boldsymbol{x}). \tag{A.7}$$

Appendix B. Analytical solution for average functions over the fiber domain for single-fiber and multi-fiber RVEs

For a second-degree polynomial homogenizing eigenstrain of the form $\epsilon^*_{mn}(\boldsymbol{x}) = H_{mn}(1 + \alpha^{sf}(x_1/a_1)^2)$ within a cylindrical fiber with length of $2a_1$ and diameter of D_f, the average function $\langle(1 + \alpha^{sf}(x_1/a_1)^2) \exp(-\mathrm{i}\boldsymbol{\xi}.\boldsymbol{x})\rangle_{\Omega}$ over the single-fiber domain required for determination of the modified Eshelby tensor in Eq. (21) can be obtained as

$$\langle(1 + \alpha^{sf}(x_1/a_1)^2) \exp(-\mathrm{i}\boldsymbol{\xi}.\boldsymbol{x})\rangle_{\Omega} = \frac{2\,J_1\left(\frac{D_f}{2}(\xi_2^2+\xi_3^2)^{1/2}\right)}{a_1\xi_1\left(\frac{D_f}{2}(\xi_2^2+\xi_3^2)^{1/2}\right)} \mathrm{Sin}[a_1\xi_1]$$

$$+\alpha^{sf}\frac{2\,J_1\left(\frac{D_f}{2}(\xi_2^2+\xi_3^2)^{1/2}\right)}{a_1^3\xi_1^3\left(\frac{D_f}{2}(\xi_2^2+\xi_3^2)^{1/2}\right)}(2a_1\xi_1\mathrm{Cos}[a_1\xi_1] + (-2 + a_1^2\xi_1^2)\mathrm{Sin}[a_1\xi_1]), \tag{B.1}$$

where J_1 represents the Bessel function of the first kind of order 1. It should be noted that the average function $\langle\exp(-\mathrm{i}\boldsymbol{\xi}.\boldsymbol{x})\rangle_{\Omega} = \langle\exp(\mathrm{i}\boldsymbol{\xi}.\boldsymbol{x})\rangle_{\Omega}$ associated with a single-fiber can be easily attained by letting α^{sf}=0 in Eq. (B.1).

For the multi-fiber RVE with the locations and involving lengths of the fibers indicated in Section 4.2, associated with the second-degree polynomial homogenizing eigenstrain of the form $\epsilon^*_{mn}(\boldsymbol{x}) = H_{mn}(1 + \alpha^{mf}(x_1/a_1)^2)$ with x_1

measured with respect to the center of each fiber, the average function $\langle(1+\alpha^{mf}(x_1/a_1)^2)\exp(-\mathrm{i}\boldsymbol{\xi}.\boldsymbol{x})\rangle_\Omega$ (average over all of the fibers within the multi-fiber RVE) required for determination of the modified Eshelby tensor in Eq. (21) is derived as

$$\langle(1+\alpha^{mf}(x_1/a_1)^2)\exp(-\mathrm{i}\boldsymbol{\xi}.\boldsymbol{x})\rangle_\Omega =$$

$$\frac{2J_1\left(\frac{D_f}{2}(\xi_2^2+\xi_3^2)^{1/2}\right)}{9a_1\xi_1\left(\frac{D_f}{2}(\xi_2^2+\xi_3^2)^{1/2}\right)}\Big(\mathrm{Sin}[a_1\xi_1]+4\mathrm{Cos}\left[\tfrac{1}{2}(a_1-2t)\xi_1\right]\mathrm{Cos}[s\xi_2]\mathrm{Sin}\left[\tfrac{a_1\xi_1}{2}\right]+\mathrm{Sin}\left[\left(\tfrac{3a_1}{2}-t\right)\xi_1+s(\xi_2-\xi_3)\right]+$$

$$\mathrm{Sin}\left[\left(\tfrac{5a_1}{4}-t\right)\xi_1-s\xi_3\right]+\mathrm{Sin}[t\xi_1-s\xi_3]+\mathrm{Sin}[t\xi_1+s\xi_2-s\xi_3]+\mathrm{Sin}\left[\left(\tfrac{3a_1}{4}-t\right)\xi_1+s\xi_3\right]+\mathrm{Sin}[t\xi_1+s\xi_3]+$$

$$\mathrm{Sin}[t\xi_1-s\xi_2+s\xi_3]+\mathrm{Sin}\left[\tfrac{1}{2}(a_1-2t)\xi_1+s(-\xi_2+\xi_3)\right]+\mathrm{Sin}\left[\tfrac{1}{4}(a_1-4t)\xi_1-s(\xi_2+\xi_3)\right]+\mathrm{Sin}[t\xi_1-$$

$$s(\xi_2+\xi_3)]+\mathrm{Sin}\left[\left(\tfrac{7a_1}{4}-t\right)\xi_1+s(\xi_2+\xi_3)\right]+\mathrm{Sin}[t\xi_1+s(\xi_2+\xi_3)]\Big)$$

$$+\alpha^{mf}\frac{2J_1\left(\frac{D_f}{2}(\xi_2^2+\xi_3^2)^{1/2}\right)}{72a_1^3\xi_1^3\left(\frac{D_f}{2}(\xi_2^2+\xi_3^2)^{1/2}\right)}\Big(8(2a_1\xi_1\mathrm{Cos}[a_1\xi_1]+(-2+a_1^2\xi_1^2)\mathrm{Sin}[a_1\xi_1])-16\Big(2(1+2\mathrm{Cos}[s\xi_2])\mathrm{Cos}[s\xi_3]\mathrm{Sin}[t\xi_1]+$$

$$2\mathrm{Cos}[s\xi_2](\mathrm{Sin}[(a_1-t)\xi_1]+\mathrm{Sin}[t\xi_1])+\mathrm{Sin}\left[\left(\tfrac{3a_1}{2}-t\right)\xi_1+s(\xi_2-\xi_3)\right]+\mathrm{Sin}\left[\left(\tfrac{5a_1}{4}-t\right)\xi_1-s\xi_3\right]+$$

$$\mathrm{Sin}\left[\left(\tfrac{3a_1}{4}-t\right)\xi_1+s\xi_3\right]+\mathrm{Sin}\left[\tfrac{1}{2}(a_1-2t)\xi_1+s(-\xi_2+\xi_3)\right]+\mathrm{Sin}\left[\tfrac{1}{4}(a_1-4t)\xi_1-s(\xi_2+\xi_3)\right]+$$

$$\mathrm{Sin}\left[\left(\tfrac{7a_1}{4}-t\right)\xi_1+s(\xi_2+\xi_3)\right]\Big)+4a_1\xi_1\Big(4\mathrm{Cos}\left[\left(\tfrac{5a_1}{4}-t\right)\xi_1-s\xi_3\right]-\mathrm{Cos}[t\xi_1-s\xi_3]+8\mathrm{Cos}[(a_1-t)\xi_1]\Big(\mathrm{Cos}[s\xi_2]+$$

$$\mathrm{Cos}\left[\tfrac{a_1\xi_1}{2}+s\xi_2-s\xi_3\right]\Big)+4\mathrm{Cos}\left[\left(\tfrac{3a_1}{4}-t\right)\xi_1+s\xi_3\right]+\mathrm{Cos}[t\xi_1+s\xi_3]+4\mathrm{Cos}\left[\tfrac{1}{4}(a_1-4t)\xi_1-s(\xi_2+\xi_3)\right]+$$

$$3\mathrm{Cos}[t\xi_1-s(\xi_2+\xi_3)]+4\mathrm{Cos}\left[\left(\tfrac{7a_1}{4}-t\right)\xi_1+s(\xi_2+\xi_3)\right]-3\mathrm{Cos}[t\xi_1+s(\xi_2+\xi_3)]+4\mathrm{Sin}[t\xi_1]\mathrm{Sin}[s(\xi_2-\xi_3)]\Big)+$$

$$a_1^2\xi_1^2\Big(16\mathrm{Cos}[s\xi_2]\mathrm{Sin}[(a_1-t)\xi_1]+(4\mathrm{Cos}[s(\xi_2-\xi_3)]+\mathrm{Cos}[s\xi_3]+9\mathrm{Cos}[s(\xi_2+\xi_3)])\mathrm{Sin}[t\xi_1]+$$

$$8\Big(\mathrm{Sin}\left[\left(\tfrac{3a_1}{2}-t\right)\xi_1+s(\xi_2-\xi_3)\right]+\mathrm{Sin}\left[\left(\tfrac{5a_1}{4}-t\right)\xi_1-s\xi_3\right]+\mathrm{Sin}\left[\left(\tfrac{3a_1}{4}-t\right)\xi_1+s\xi_3\right]+\mathrm{Sin}\left[\tfrac{1}{2}(a_1-2t)\xi_1+$$

$$s(-\xi_2+\xi_3)\right]+\mathrm{Sin}\left[\tfrac{1}{4}(a_1-4t)\xi_1-s(\xi_2+\xi_3)\right]+\mathrm{Sin}\left[\left(\tfrac{7a_1}{4}-t\right)\xi_1+s(\xi_2+\xi_3)\right]\Big)\Big)\Big), \qquad \text{(B.2)}$$

in which $t=L_1$ and $s=2L_2/3$ (note that $L_2=L_3$ for the considered multi-fiber RVE). Subsequently, the average function $\langle\exp(-\mathrm{i}\boldsymbol{\xi}.\boldsymbol{x})\rangle_\Omega=\langle\exp(\mathrm{i}\boldsymbol{\xi}.\boldsymbol{x})\rangle_\Omega$ associated with the multi-fiber RVE can be attained by letting α^{mf}=0 in Eq. (B.2).

References

Ahmadi, H., Hajikazemi, M., Van Paepegem, W., 2020. Closed-form formulae for prediction of homogenized ply-properties and laminate thermo-elastic constants in symmetric laminates containing ply cracks in multiple orientations. Composite Structures 241, 112061.

Arif, M.F., Meraghni, F., Chemisky, Y., Despringre, N., Robert, G., 2014. In situ damage mechanisms investigation of PA66/GF30 composite: Effect of relative humidity. Composites Part B: Engineering 58, 487-495.

Benveniste, Y., 1987. A new approach to the application of Mori-Tanaka's theory in composite materials. Mechanics of materials 6, 147-157.

Digimat, 2011. Software for the Linear and Nonlinear Multi-Scale Modeling of Heterogeneous Materials; e-Xstream Engineering: Louvain-la-Neuve. Belgium.

Eshelby, J.D., 1957. The determination of the elastic field of an ellipsoidal inclusion, and related problems. Proceedings of the royal society of London. Series A. Mathematical and physical sciences 241, 376-396.

Fu, S.-Y., Lauke, B., Mäder, E., Yue, C.-Y., Hu, X., 2000. Tensile properties of short-glass-fiber-and short-carbon-fiber-reinforced polypropylene composites. Composites Part A: Applied Science and Manufacturing 31, 1117-1125.

Garoz, D., Gilabert, F., Sevenois, R., Spronk, S., Van Paepegem, W., 2019. Consistent application of periodic boundary conditions in implicit and explicit finite element simulations of damage in composites. Composites Part B: Engineering 168, 254-266.

Gusev, A.A., 2016. Controlled accuracy finite element estimates for the effective stiffness of composites with spherical inclusions. International journal of solids and structures 80, 227-236.

Jain, A., Lomov, S.V., Abdin, Y., Verpoest, I., Van Paepegem, W., 2013. Pseudo-grain discretization and full Mori Tanaka formulation for random heterogeneous media: Predictive abilities for stresses in individual inclusions and the matrix. Composites science and technology 87, 86-93.

Karsli, N.G., Aytac, A., 2013. Tensile and thermomechanical properties of short carbon fiber reinforced polyamide 6 composites. Composites Part B: Engineering 51, 270-275.

Khezrzadeh, H., 2017. A statistical micromechanical multiscale method for determination of the mechanical properties of composites with periodic microstructure. Composites Part B: Engineering 115, 138-143.

McCartney, L., 2010. Maxwell's far-field methodology predicting elastic properties of multiphase composites reinforced with aligned transversely isotropic spheroids. Philosophical Magazine 90, 4175-4207.

McCartney, L.N., Kelly, A., 2008. Maxwell's far-field methodology applied to the prediction of properties of multi-phase isotropic particulate composites. Proceedings of the Royal Society A: Mathematical, Physical and Engineering Sciences 464, 423-446.

Mirkhalaf, S., Eggels, E., van Beurden, T., Larsson, F., Fagerström, M., 2020. A finite element based orientation averaging method for predicting elastic properties of short fiber reinforced composites. Composites Part B: Engineering 202, 108388.

Molnár, S., Rosenberger, S., Gulyás, J., Pukánszky, B., 1999. Structure and impact resistance of short carbon fiber reinforced polyamide 6 composites. Journal of Macromolecular Science—Physics 38, 721-735.

Mori, T., Tanaka, K., 1973. Average stress in matrix and average elastic energy of materials with misfitting inclusions. Acta metallurgica 21, 571-574.

Mura, T., 2013. Micromechanics of defects in solids. Springer Science & Business Media.

Naili, C., Doghri, I., Kanit, T., Sukiman, M., Aissa-Berraies, A., Imad, A., 2020. Short fiber reinforced composites: Unbiased full-field evaluation of various homogenization methods in elasticity. Composites Science and Technology 187, 107942.

Nemat-Nasser, S., Hori, M., 2013. Micromechanics: overall properties of heterogeneous materials. Elsevier.

Nemat-Nasser, S., Iwakuma, T., Hejazi, M., 1982. On composites with periodic structure. Mechanics of materials 1, 239-267.

Nemat-Nasser, S., Taya, M., 1981. On effective moduli of an elastic body containing periodically distributed voids. Quarterly of Applied Mathematics 39, 43-59.

Nomura, S., Chou, T.-W., 1984. Bounds for elastic moduli of multiphase short-fiber composites. Journal of Applied Mechanics 51, 540-545.

Pettermann, H., Böhm, H.J., Rammerstorfer, F.G., 1997. Some direction-dependent properties of matrix-inclusion type composites with given reinforcement orientation distributions. Composites Part B: Engineering 28, 253-265.

Rashidinejad, E., Naderi, A.A., 2018. Analytical study of electro-elastic fields in quantum nanostructure solar cells: the inter-nanostructure couplings and geometrical effects. Acta Mechanica 229, 3089-3106.

Rashidinejad, E., Shodja, H.M., 2019. On the exact nature of the coupled-fields of magneto-electro-elastic ellipsoidal inclusions with non-uniform eigenfields and general anisotropy. Mechanics of Materials 128, 89-104.

Rashidinejad, E., Shodja, H.M., 2020. Novel theories on magneto-electro-elastic ellipsoidal multi-inclusions and inhomogeneities and associated impotent fields. Mechanics of Materials 143, 103201.

Sato, N., Kurauchi, T., Sato, S., Kamigaito, O., 1991. Microfailure behaviour of randomly dispersed short fibre reinforced thermoplastic composites obtained by direct SEM observation. Journal of materials science 26, 3891-3898.

Shodja, H.M., Rashidinejad, E., 2014. Interacting functionally graded quantum wires/quantum dots with arbitrary shapes and general anisotropy within a distinct piezoelectric matrix. Journal of the Mechanical Behavior of Materials 23, 1-14.

Shodja, H.M., Roumi, F., 2005. Overall behavior of composites with periodic multi-inhomogeneities. Mechanics of Materials 37, 343-353.

Soden, P.D., Hinton, M.J., Kaddour, A.S., 2004. Lamina properties, lay-up configurations and loading conditions for a range of fibre reinforced composite laminates, Failure Criteria in Fibre-Reinforced-Polymer Composites. Elsevier, pp. 30-51.

Tucker III, C.L., Liang, E., 1999. Stiffness predictions for unidirectional short-fiber composites: review and evaluation. Composites science and technology 59, 655-671.

Wu, L., Noels, L., Adam, L., Doghri, I., 2013. A combined incremental-secant mean-field homogenization scheme with per-phase residual strains for elasto-plastic composites. International Journal of Plasticity 51, 80-102.

Wu, L., Sket, F., Molina-Aldareguia, J.M., Makradi, A., Adam, L., Doghri, I., Noels, L., 2015. A study of composite laminates failure using an anisotropic gradient-enhanced damage mean-field homogenization model. Composite Structures 126, 246-264.